

Journal Pre-proof

Investigation on strengthening and toughening mechanisms of Nb-Ti-ZrB₂ metal matrix ceramic composites reinforced with in situ niobium and titanium boride



Yuan Gao, Zongde Liu, Qing Wang, Congcong Liu, Youmei Sun

PII: S0263-4368(20)30158-X

DOI: <https://doi.org/10.1016/j.ijrmhm.2020.105282>

Reference: RMHM 105282

To appear in: *International Journal of Refractory Metals and Hard Materials*

Received date: 4 April 2020

Revised date: 8 May 2020

Accepted date: 11 May 2020

Please cite this article as: Y. Gao, Z. Liu, Q. Wang, et al., Investigation on strengthening and toughening mechanisms of Nb-Ti-ZrB₂ metal matrix ceramic composites reinforced with in situ niobium and titanium boride, *International Journal of Refractory Metals and Hard Materials* (2019), <https://doi.org/10.1016/j.ijrmhm.2020.105282>

This is a PDF file of an article that has undergone enhancements after acceptance, such as the addition of a cover page and metadata, and formatting for readability, but it is not yet the definitive version of record. This version will undergo additional copyediting, typesetting and review before it is published in its final form, but we are providing this version to give early visibility of the article. Please note that, during the production process, errors may be discovered which could affect the content, and all legal disclaimers that apply to the journal pertain.

© 2019 Published by Elsevier.

Investigation on strengthening and toughening mechanisms of Nb-Ti-ZrB₂ metal matrix ceramic composites reinforced with in situ niobium and titanium boride

Yuan Gao^{1,a}, Zongde Liu^{1,b,*}, Qing Wang^{2,c}, Congcong Liu^{1,d}, Youmei Sun^{1,e}

¹Key Laboratory of Energy Transfer and System of Power Station of Ministry of Education, North China Electric Power University, Beijing 102206, China

²Department of Engineering, Durham University, Durham DH1 3LE, UK

^{b,*}Corresponding author: Zongde Liu, Professor, PhD. Telephone: +86-18515435590, E-mail: lzd@ncepu.edu.cn, Postal address: No.2 Beinong Road, Huilongguan Town, Changping District, Beijing, North China Electric Power University, Beijing 102206, China; ^aemail: 18810178944@163.com; ^cemail: qing.wang@durham.ac.uk; ^demail: jyfcc5613@163.com; ^eemail: sunyoumei_123@163.com;

Abstract

Nb-Ti-ZrB₂ metal matrix ceramic composites with a fixed atomic ratio Nb/Ti=2/1 and ZrB₂ volume fraction changing from 0, 11 vol.%, 23 vol.% to 36 vol.% were hot pressed at 1600°C under 30 MPa. The influence of ZrB₂ content and Ti addition on the phase constitution, microstructure evolution, toughening mechanisms and strengthening mechanisms were investigated. It was shown that the formation of in situ Nb-rich (Ti,Nb)B and Ti-rich (Nb,Ti)B was attributed to a high mutual solubility of monoborides and the amount of niobium and titanium borides increased with increasing ZrB₂ content. The needle-shaped (Ti,Nb)B phase weakened the damage to fracture toughness caused by ZrB₂ particle fracture due to crack bridging, crack deflection and the pull-out toughening mechanisms. The highest fracture

toughness of the Nb-Ti-ZrB₂ composites was 12.0 MPa·m^{1/2}. The stiff (Nb,Ti)B phase acted as a strong obstacle to the dislocation motion, leading to dislocation pile-up and enhancing the strength of the Nb-Ti-ZrB₂ composites during compression tests. However, stress concentration around the needle-shaped (Ti,Nb)B phase easily leads to crack initiation and extension, resulting in decreased strength. The yield strength of Nb-Ti-ZrB₂ composites ranged from 657.3 MPa to 1783.0 MPa owing to the combined influence of the strengthening mechanism caused by (Nb,Ti)B and the weakening mechanism caused by (Ti,Nb)B. The compressive deformation and failure process were also discussed in detail in this study.

Keywords: Hot-pressing; Nb-based composite; ZrB₂; Mechanical properties; Fracture behavior

1. Introduction

Nb alloys are the most potential high temperature structural materials due to their high melting point, good corrosion resistance and excellent refractory properties [1-3]. However, the main obstacles for them to be used widely is their low fracture toughness at room temperature. To overcome this drawback, various approaches have been used. The effect of W [4], Ta [5] and V [6] on toughening mechanism of Nb or Nb-Si alloys were investigated. Fracture toughness of the Nb-Si based alloys were improved by the addition of Ta, but reduced to 8.2 MPa·m^{1/2} by addition of W. Nb_{SS}/Nb₃Al [7] and Nb_{SS}/Nb₅Si₃ [8] were fabricated to study the effect of intermetallic compounds on the strength and toughness. A ductile/reinforcement two-phase structure is formed in the Nb_{SS}/Nb₅Si₃ composite. Nb₅Si₃ phases are the reinforcement phases which are beneficial to room temperature strength and oxidation resistance. The Nb_{SS} phase is the ductile matrix which can enhance fracture toughness and room temperature ductility [8]. However, the fracture toughness and ductility of these composites are still too low to be used

in the industry [9].

Particulate reinforced metal matrix composites (PRMMCs) are being considered as potential materials for aerospace owing to their high wear resistance, good balance between strength and toughness, and low thermal expansion [10]. Moreover, the PRMMCs can be fabricated with near isotropic properties in three orthogonal directions compared with the fiber or filament reinforced composites [11]. Many studies have focused on metal matrix composites reinforced with Nb particles [12, 13], but there haven't been any reports on the ceramic particulate reinforced Nb based composites. In previous studies of our team, the (0-60 vol%) ZrB₂ particles reinforced NbMoss solid solution matrix composites were fabricated by hot-press sintering at 2400°C [14, 15]. The experimental results show that the ZrB₂ ceramic particles can significantly improve the compressive strength of the NbMoss matrix. The highest compressive strength at room temperature reached 1635.91 MPa, and the strength at 1300 °C is still over 700 MPa. However, their room temperature fracture toughness is only 3.99-6.34 MPa·m^{1/2}, restricting their practical application. It is necessary to adjust the chemical element composition to obtain a good ductility and a high fracture toughness of the ZrB₂ particles reinforced Nbss composite when maintaining its high compressive strength.

One of the most promising approaches to enhance the fracture toughness of particulate reinforced Nb composites is to weaken the negative effect of the ceramic reinforcement brittleness fracture by crack deflection and crack bridges provided by a ductile metal matrix [16, 17]. It has been demonstrated that the addition of Ti can improve the ductility of the Nb [18, 19]. The fracture toughness of Nb-15Al-Ti alloys increases from 27 MPa·m^{1/2} to 102 MPa·m^{1/2} while Ti content increases from 10 at.% to 40 at.% due to the effects of TiO₂-induced closure

[20]. Consequently, ZrB_2 was selected as the reinforced particles and Ti was added into Nb to form the NbTi solid solution matrix to provide toughness and ductility in this work. As for the processing techniques, hot pressing is a more feasible method for processing refractory Nb-based composites with finer microstructures and better compositional homogeneity than vacuum arc melting or casting [11, 21]. During hot-press sintering, the ZrB_2 particles have the possibility of decomposing into Zr and B and then B can react with Nb and Ti to form the in-situ NbB and/or TiB. According to the study of D. B. Borisov et al. [22], the phase composition of the Nb-Ti-B alloy is composed of three phase NbTi₃+Nb₂B+TiB when the Nb/Ti is approximately 2/1 (atomic ratio). NbB and TiB are also excellent reinforced particles to Nb alloys due to the combination of high specific strength and high temperature resistance [23]. In this study, the atomic ratio of Nb/Ti was chosen as 2/1 and Nb-Ti-x ZrB_2 (x=0, 11, 23, 36vol.%) composites were hot pressed at 1600°C under 30 MPa. The phase composition and microstructures evolution were investigated. The compressive yield strength, fracture toughness and fracture morphologies were examined and the related strengthening mechanism and toughening mechanism were discussed in detail.

2. Materials and Methods

2.1 Samples fabrication

The raw materials are ZrB_2 (23 μ m, purity>99.95%), Nb (18-25 μ m, purity> 99.95%) and Ti (45 μ m, purity> 99.95%) powders provided by Beijing gold crown new material Technology Co., Ltd. China. Four powder mixtures (Table 1) with different ZrB_2 volume fraction were mixed and pulverized in a planetary ball mill in ethanol for 12 h at a speed of 200 rpm. Then the mixtures were dried at 110 °C for 3 h and uniaxially cold-pressed into platelets under a pressure

of 10 MPa. Subsequently, the platelet was put into a carbon die with BN coating in a vacuum hot press furnace and the hot-press sintering process started. At the first stage of the sintering process, the heating rate was $10^{\circ}\text{C min}^{-1}$ and vacuum degree was ~ 1.5 Pa. The first dwell isotherm was 10 min at 400°C . The volatile species in the sample could be removed during this stage. At the second stage, the heating rate was $20^{\circ}\text{C min}^{-1}$ and vacuum degree was ~ 0.2 Pa. The second dwell isotherm was 2 h at 1600°C and a pressure of 30 MPa was supplied during the dwell time. In the end, the compact was naturally cooled down in the hot press furnace. One billet, with dimensions of $36 \times 25 \times 20$ mm³, was prepared for each experiment.

Table 1 Raw materials compositions

Sample	Atomic ratio			ZrB ₂ volume fraction (%)
	ZrB ₂	Nb	Ti	
Z0	—	2	1	0
Z1	0.4	2	1	11
Z2	0.9	2	1	23
Z3	1.7	2	1	36

2.2 Mechanical property evaluation

Fracture toughness test specimens with dimensions of $3\text{mm} \times 4\text{mm} \times 36\text{mm}$ were prepared from the hot-pressed compacts by electro-discharge machining and the notch at mid-length was 0.1 mm wide and 0.6 mm deep according to GB/T 23806-2009. Compression test specimens of 10mm in height and 10mm in diameter were also prepared according to GB/T 7314-2005. SiC sandpapers from #100 to #800 were used to grind the specimens. The fracture toughness value was determined by a three point bending test using the single-edge-notched beam (SENB) specimens by an Electromechanical Universal Testing Machine (C45.105). The surfaces obtained from the Indentation Method (IM) were also investigated to show the crack propagation pathways. The final result is the average of five specimens. The compression tests

were conducted on a hydraulic universal machine (SHT 4305) operating under a load control of 600 N/s. The loading direction was set to be perpendicular to the hot-pressing direction.

2.3 Microstructure characterization

The phase identification was performed on bulk samples using a Rigaku D/max-rA X-ray diffract meter with Cu $K\alpha$ radiation, between 2θ angles of 10° and 90° at a scanning rate of $8^\circ/\text{min}$. The microstructures were examined on a FESEM scanning electron microscope (ZEISS SUPRA-55) equipped with an EDAX genesis xm-2 X-ray spectrometer. The surfaces of specimens for Vickers hardness, X-ray diffraction analysis and microstructure observation were grinded and polished.

3. Result

3.1 Phase and microstructure

XRD patterns of the Nb-Ti-ZrB₂ composites are displayed in Fig. 1. Peaks from the (Ti,Nb,Zr)_{ss}, TiB, NbB and ZrB₂ phases are detected. The intensity of the niobium boride peaks increases with increasing ZrB₂ volume fraction in the corresponding XRD profiles, indicating the amount of TiB and NbB phases increases. For Z1, Z2, Z3 samples, the formation of the β (Ti,Nb,Zr)_{ss} solid solution is mainly due to the solution of Ti and Zr atoms into a Nb crystal lattice. It should be noted that the concentration of Ti is ~ 22.28 at.% for NbB and the concentration of Nb is ~ 24.88 at.% for TiB, indicating the existence of Ti-rich (Nb,Ti)B and Nb-rich (Ti,Nb)B (see Table 2 for details). (Nb,Ti)B and (Ti,Nb)B phases are also found in the annealed Ti-Nb-B alloys by D. B. Borisov [22]. In his study, the solubility of Nb in TiB is up to 23 at.% and the highest solubility of Ti in NbB is 15 at.%. Ding et al. [24] found that only the single β (Ti,Nb)_{ss} phase appeared in the Nb-based alloy when the addition

of Ti was less than 35 at.%. This is the reason why only the $\beta(\text{Ti,Nb})\text{ss}$ phase is detected in Z0.

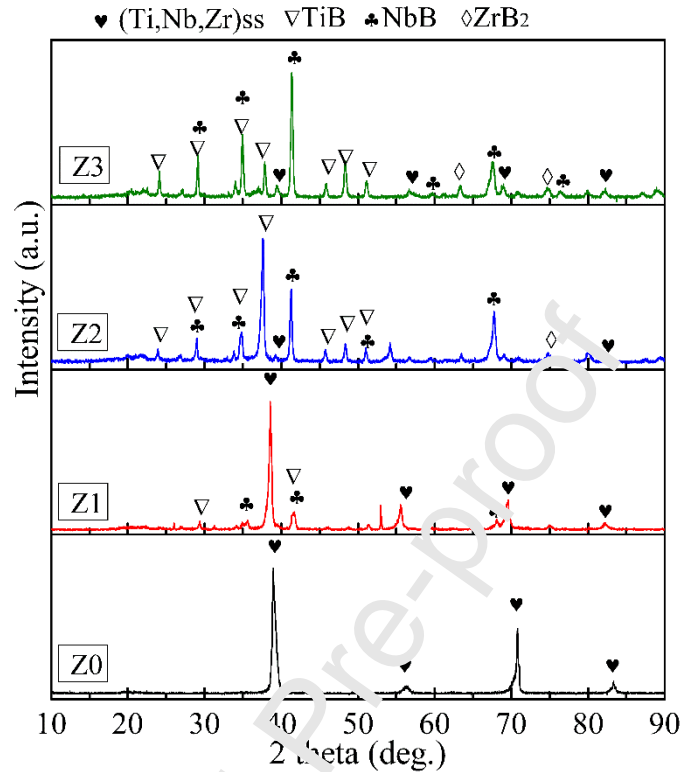


Fig. 1. XRD patterns for Nb-Ti-ZrB₂ composites after hot-press sintering at 1600°C.

The microstructure and EDX results of the $\beta(\text{Ti,Nb,Zr})\text{ss}$, Ti-rich (Nb,Ti)B, Nb-rich (Ti,Nb)B and ZrB₂ phases in Z1-Z3 are shown in Fig. 2 and Table 2. Arrows A_i , B_i , C_i and D_i ($i=1, 2, 3$) indicate different phases with different atomic compositions. Phase A_i is the (Nb,Ti,Zr)ss solid solution phase containing Nb, Ti, Zr and B without a stoichiometric composition. Phase B_i is the Nb-rich (Ti,Nb)B phase with a stoichiometric composition quite close to TiB and the concentration of Nb in Z1, Z2 and Z3 is 21.64 at.%, 24.88 at.% and 17.01 at.%, as indicated by arrows B1, B2 and B3, respectively. Phase C_i is the Ti-rich (Nb,Ti)B phase containing 18.18 at.%, 22.28 at.% and 17.92 at.% Ti, as indicated by arrows C1, C2 and C3, respectively. The high solubility of Ti in NbB (~30 at.%) and of Nb in TiB (~23 at.%) has also been observed by G. V. Samsonov et al. before [22, 25, 26]. ZrB₂ is detected in Z2 and Z3

according to XRD patterns; however, the SEM image and EDX analysis show that only Z3 exhibits large residual ZrB_2 particles, as indicated by D3. The amount of ZrB_2 in Z2 is too small to be distinguished by a scanning electron microscope due to its the limited resolution. In general, the EDX element analysis is consistent with the phase constitution identified by the XRD patterns.

Fig. 2 shows the typical images of the polished Nb-Ti- ZrB_2 composites. The needle-shaped (Ti,Nb)B [23], the nearly spherical NbB [22] and the polygonal shaped ZrB_2 [14] are displayed in the (Ti,Nb,Zr)ss solid solution matrix. During the hot-pressing process, the ZrB_2 particles firstly decompose into Zr and B, and then B reacts with Ti by an in situ chemical reaction $Ti+B=TiB$ to precipitate an intermetallic TiB phase [27]. TiB phase usually grows along the [010] direction and presents a needle-shaped or rod-like morphology due to its B27 crystal structure [23, 28]. The formation of β (Ti,Nb,Zr)ss and NbB phases is due to the eutectic reaction $L \leftrightarrow Nbss+NbB$ [29], and the formation of (Ti,Nb)B and (Nb,Ti)B is due to the high mutual solubility of NbB and TiB [23]. However, the decomposition of ZrB_2 is incomplete as there are residual polygonal-shaped ZrB_2 particles distributed in the (Ti,Nb,Zr)ss matrix of Z3 (Fig. 2c and c1). Moreover, with increasing ZrB_2 content in the raw material, more and more (Ti,Nb)B whiskers are synthesized through the above chemical reaction, then the resulting (Ti,Nb)B grows and connects rapidly to form the (Ti,Nb)B cluster (Fig. 2a-c). The amount of (Ti,Nb)B cluster increases with increasing ZrB_2 volume fraction in the raw material. Both the (Ti,Nb)B cluster and the polygonal ZrB_2 can cause stress concentration, causing a negative influence on the compressive properties of the investigated Nb-Ti- ZrB_2 composites, which will be discussed in section 4.2.

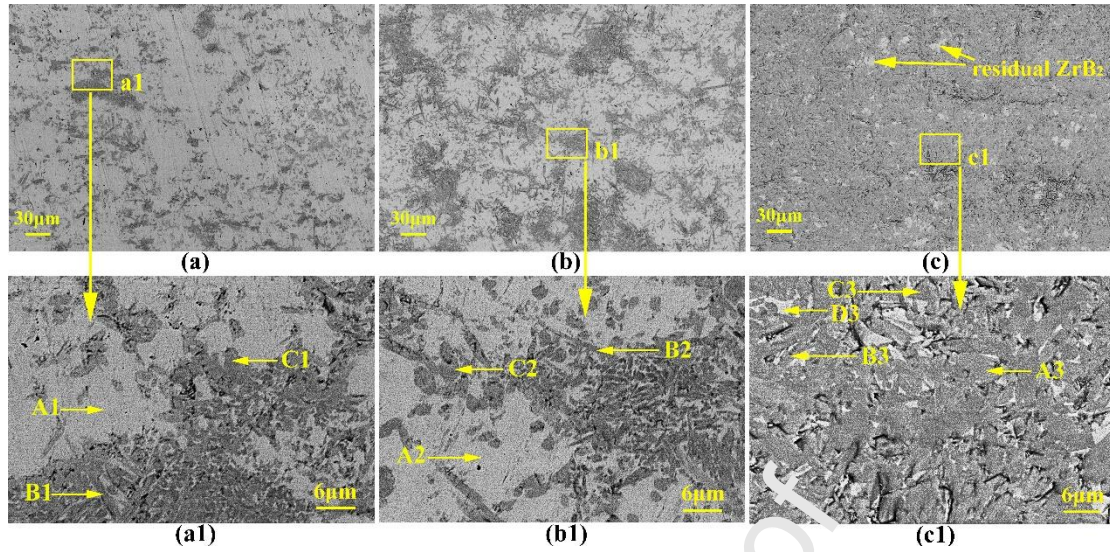


Fig. 2. Microstructure of Nb-Ti-ZrB₂ composites: (a)Z1, (b)Z2 (c)Z3, (a1)Magnification of Z1, (b1)Magnification of Z2, (c1)Magnification of Z3

Table 2 EDS results for the typical phases in Fig. 2

Sample	Arrow	Composition (at.%)				Constituent phases
		Nb	Ti	Zr	B	
Z1	A1	29.05	35.15	6.86	28.94	(Nb,Ti,Zr)ss
	B1	21.64	25.34	4.83	48.18	Nb-rich (Ti,Nb)B
	C1	28.79	33.18	1.79	51.25	Ti-rich (Nb,Ti)B
Z2	A2	24.62	21.19	17.26	37.46	(Nb,Ti,Zr)ss
	B2	24.38	24.74	4.66	45.71	Nb-rich (Ti,Nb)B
	C2	25.03	22.28	6.42	45.26	Ti-rich (Nb,Ti)B
Z3	A3	13.30	14.43	33.53	38.73	(Nb,Ti,Zr)ss
	B3	17.01	24.19	10.12	48.68	Nb-rich (Ti,Nb)B
	C3	22.48	17.92	6.92	52.68	Ti-rich (Nb,Ti)B
	D3	2.35	3.50	38.44	55.71	ZrB ₂

3.2 Fracture toughness

The fitting curve of fracture toughness versus ZrB₂ volume fraction for the Nb-Ti-ZrB₂ composites is shown in Fig. 3. It can be seen that the addition of ZrB₂ particles decreases fracture toughness of Nb-Ti alloys compared to Z1-Z3 with Z0. The addition of ceramic particles to alloys causing a decrease in fracture toughness is also observed in other PMMCs such as Al₂O₃/SiC/TiB₂ reinforced Al/Ti matrix composites. This phenomenon is due to the

restrained plastic deformation of the matrix caused by the stiff particles [30] and particle fracture, particle clustering, and particle/matrix debonding [31, 32]. Rice and Johnson [33] indicate that the toughness should decrease as a function of the particulate volume fraction to the power $-1/6$. This is substantiated by the present results, as shown in Fig. 3 and Table 3.

However, the fracture toughness of Z2 is an exception to the Rice and Johnson rule. This phenomenon is mainly due to three toughening mechanisms caused by the needle-shaped (Ti,Nb)B phase, which will be discussed in detail in section 4.1

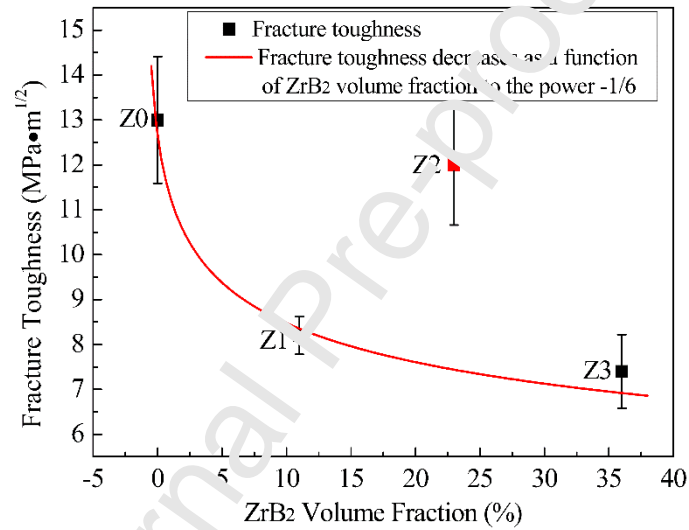


Fig. 3. Fitting curve of fracture toughness versus ZrB₂ volume fraction for the Nb-Ti-ZrB₂ composites.

Table 3 Mechanical properties of Nb-Ti-(ZrB₂) composites

Sample	Fracture toughness (MPa·m ^{1/2})	Yield strength (MPa)
Z0	13.0±1.4	1252.7±70.4
Z1	8.2±0.4	1785.6±116.3
Z2	12.0±1.3	1461.4±49.6
Z3	7.4±0.8	805.1±30.9

3.3 Compressive properties

The true compressive stress-strain curves of the Nb-Ti-ZrB₂ composites are shown in Fig. 4

and Table 3 summarizes their compressive yield strength at 0.2% plastic compressive strain. It can be seen that Z1-Z3 experience brittleness deformation while Z0 displays plastic deformation with good ductility. Generally, the addition of ZrB_2 ceramic particles into an Nb-Ti alloy matrix can improve yield strength of Nb-Ti- ZrB_2 composites. This phenomenon is due to the secondary phase strengthening mechanism, which can be described as $\Delta\sigma = V_p \sigma_m \left[\frac{(l+t)A}{4l} \right]$ [34, 35], where the yield stress increment $\Delta\sigma$ is proportional to matrix yield stress σ_m and particulates volume fraction V_p . $\left[\frac{(l+t)A}{4l} \right]$ is a constant related to the size and thickness of the particulate. According to the above equation, the yield stress increment ($\Delta\sigma$) increases with increasing hard particulates. The secondary phase strengthening mechanism has also been confirmed in the other Nb based composites, such as Nb-Mo-ZrC [36] and Nb-Ti-C-B [37] composites. However, in this study, the yield strength of Nb-Ti- ZrB_2 composites decreases with increasing ZrB_2 particles, although the amount of stiffening secondary phase Ti-rich (Nb,Ti)B and Nb-rich (Ti,Nb)B increases with increasing ZrB_2 particles (Fig. 5). This phenomenon is mainly due to the stress concentration around the needle-shaped (Ti, Nb)B phases and the large residual ZrB_2 particles. The detailed weakening mechanism and the deformation behavior of Nb-Ti- ZrB_2 composites will be discussed in section 4.2.

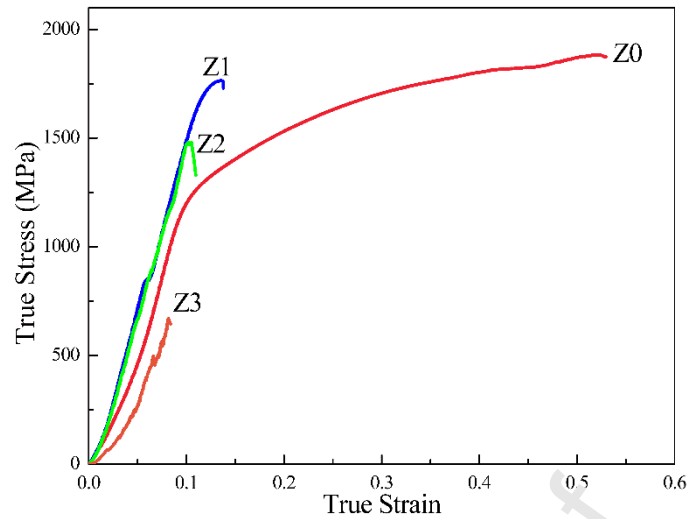


Fig. 4. True stress-strain curves for Nb-Ti-(ZrB₂) composites.

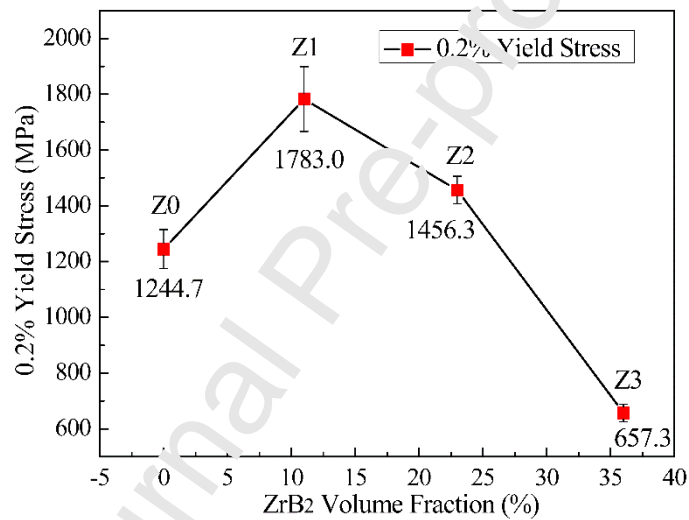


Fig. 5. 0.2% Yield strength of Nb-Ti-ZrB₂ composites.

4. Discussion

4.1 Toughening mechanism and fractography

The deformation behavior of Nb-Ti-ZrB₂ composites is different from that of ductile alloys and brittle ceramics [38]. To explore the toughening mechanisms of Nb-Ti-ZrB₂ composites, the paths of Vickers-indentation-caused cracks of Z2 and Z3 were observed on Fig. 6. As shown in Fig. 6c and d, the crack bridging and deflection occurs around the needle-shaped (Ti,Nb)B phases. The difference in elastic modulus between the (Ti,Nb)B phase and the β (Ti,Nb,Zr)ss

solid solution phase leads to the interaction between phase boundaries and crack tips, resulting in the tortuous pathway of the crack propagation (Fig. 6a). Once the cracks have reached the interfaces between the stiff (Ti,Nb)B reinforced phase and ductile β (Ti,Nb,Zr)ss matrix, the different crack-tip opening displacement between the brittle reinforcement and the ductile matrix leads to the crack bluntness and circumvention around the stiff (Ti,Nb)B phase. Consequently, the higher (Ti,Nb)B content results in a higher possibility of crack bridging and deflection.

Crack bridging and deflection can reduce the crack-tip stress intensity factor and cause energy dissipation, which is beneficial for toughening brittle materials [18, 39]. However, the crack was across the big residual ZrB_2 particles directly in Z3 (Fig. 6d), indicating the big residual ZrB_2 particle in the crack propagation path had a negative effect on crack bridging and deflection. This phenomenon is also observed on the study of SiC- ZrB_2 composites reported by Guo et al. [40]. In their study, the crack deflection and bridging appeared only at the small stiff SiC particles rather than the large ones. Therefore, the reason for the low fracture toughness of Z3 with higher (Ti,Nb)B content when compared with Z2 is the existence of the big residual ZrB_2 particles, which makes cracks cross directly rather than bridge or deflect.

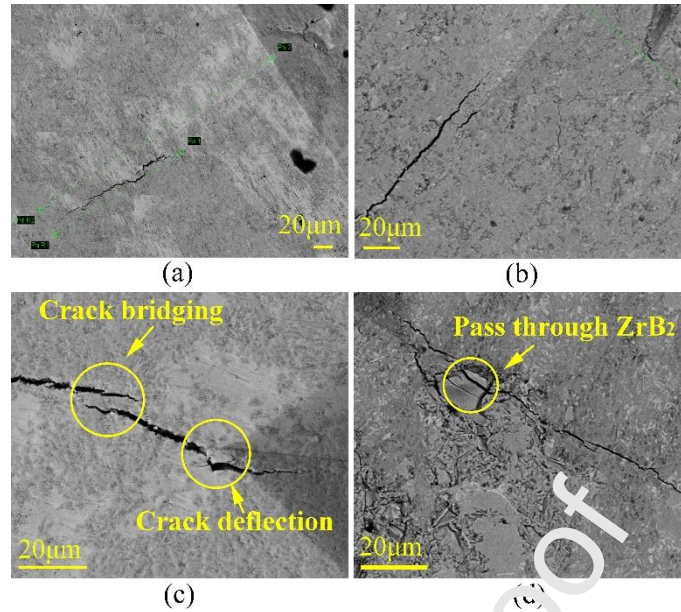


Fig. 6. Crack propagation pathways of Nb-Ti-ZrB₂ composites: (a)Z2, (b)Z3, (c)high magnification of Z2, (d)high magnification of Z3.

The fracture surfaces of Nb-Ti-ZrB₂ composites are shown in Fig. 7. Three different fracture modes were observed in Fig. 7: quasi-cleavage of the (Ti,Nb,Zr)ss, cleavage of the (Nb,Ti)B, and pull-out of the (Ti,Nb)B. Quasi-cleavage fracture occurred in the (Ti,Nb,Zr)ss solid solution matrix with obvious river patterns [41, 42]. Cleavage fracture takes place in the grains of (Nb,Ti)B with rough cleavage planes and the transgranular fracture surfaces. Pull-out of the needle-shaped (Ti,Nb)B on the crack surface of Z2 is positive for crack bridging [42], which is in agreement with the crack path propagation shown in Fig. 6c. The fine and needle-shaped (Ti,Nb)B phase results in more grain boundaries to hinder the crack propagation, and the pull-out of (Ti,Nb)B phases absorbs much of the crack expansion energy [28]. The microcracks and deflects in the Nb-Ti-ZrB₂ composites were initiated and expanded under the external loading, and finally fractured with obvious river patterns around the stiff phases. This fracture process is reasonably speculated from the fracture surfaces shown in Fig. 7. Rising R-curves

would be generated, which is consistent with these fracture surfaces [43, 44]. Related research about the influence of phase composition and microstructure on the shape of R-curves will be conducted in the future.

In general, there is no doubt that the addition of ZrB_2 particles causes the decrease in fracture toughness of Nb-Ti- ZrB_2 composites due to the restrained plastic deformation of the matrix and the brittle transgranular fracture of ZrB_2 . However, the (Ti,Nb)B phase is beneficial to fracture toughness due to crack bridging, crack deflection and the pull-out toughening mechanism. The increase of fracture toughness caused by (Ti,Nb)B in Z2 exceeds the decrease in fracture toughness caused by the ZrB_2 fracture. That is the reason for the high fracture toughness of Z2. Toughening mechanisms of the (Ti,Nb)B phase can be described schematically, as shown in Fig.

8.

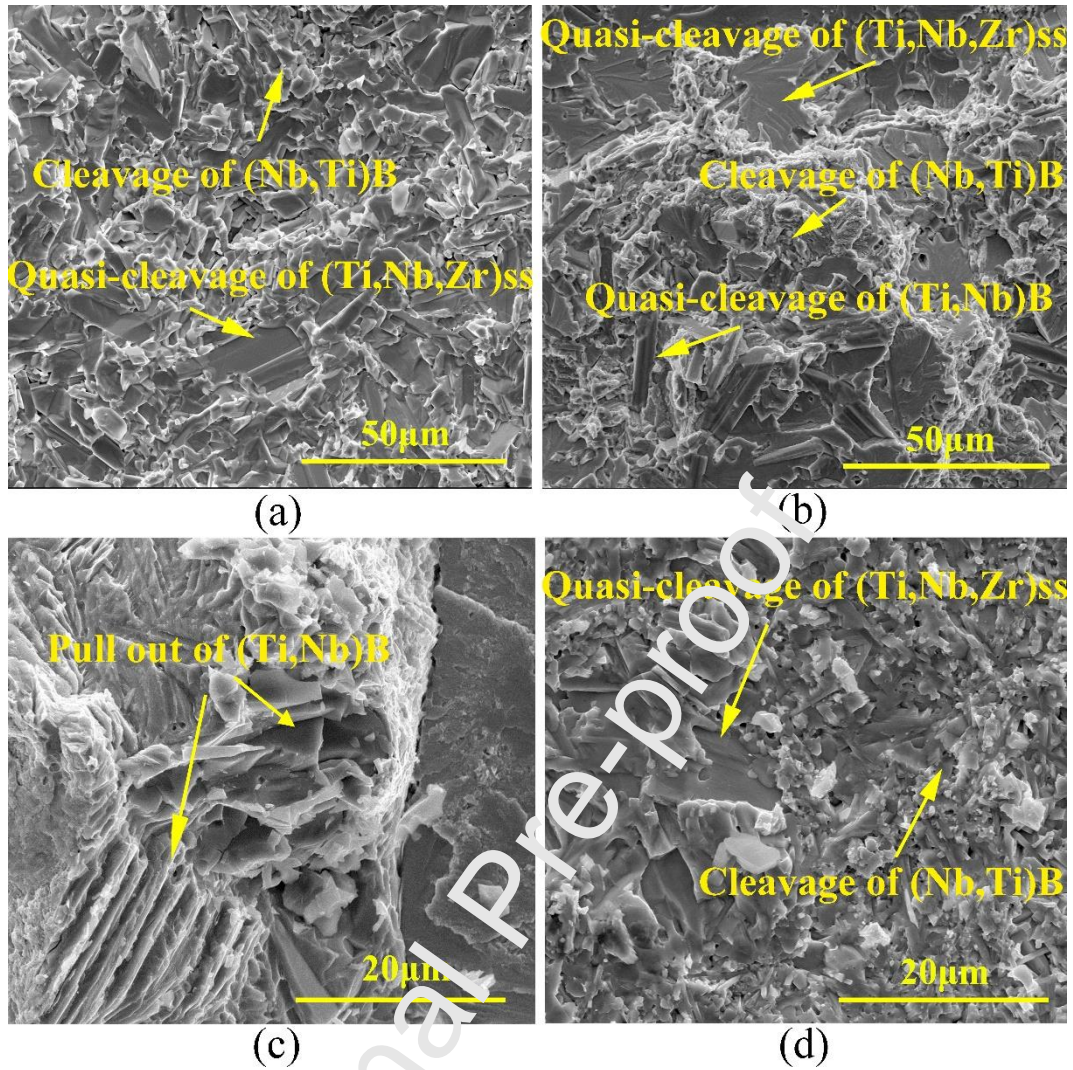


Fig. 7. Fracture surface of Nb-Ti-ZrB₂ composites: (a)Z1, (b)Z2, (c)high magnification of Z2, (d)Z3.

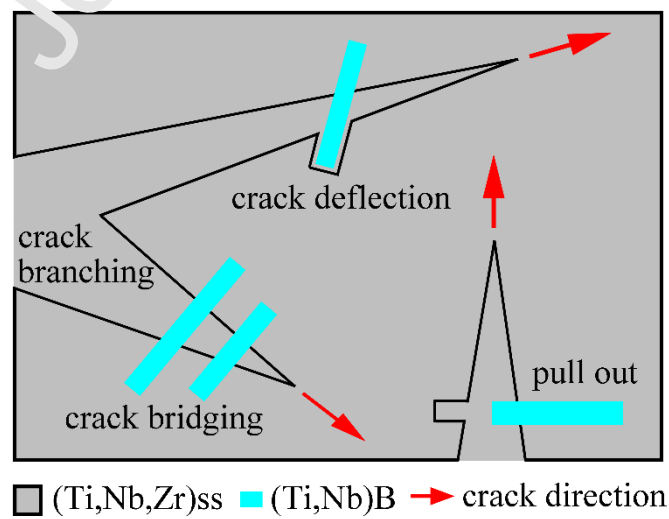


Fig. 8. Schematic diagram of toughening mechanisms of (Ti,Nb)B phase.

4.2 Strengthening mechanism and failure process

As shown in Fig. 1 and Fig. 2, there are three different hard phases: (Nb,Ti)B, (Ti, Nb)B and residual ZrB_2 particles distributed in the plastic (Ti,Nb,Zr)ss solid solution matrix in the Nb-Ti-ZrB₂ composites. During compression tests, the (Nb,Ti)B stiffening phase was a strong obstacle for the dislocation motion. The dislocations were piled up around the (Nb,Ti)B phase, which is beneficial to the improvement of the strength of Nb-Ti-ZrB₂ composites. The strengthening effect caused by the (Nb,Ti)B phase is also reported by X.J. Zhang et al [45]. However, there are two negative factors caused by the existence of the needle-shaped (Ti, Nb)B phase and the big residual ZrB_2 particles, which do harm to the compressive strength in the investigated Nb-Ti-ZrB₂ composites. First, the stress concentration around the needle-shaped (Ti, Nb)B phase easily leads to crack initiation and propagation with less compatible deformation, resulting in decreased strength during composite deformation [46]. It has been proved that the adhesion strength between the needle-shaped (Ti,Nb)B phase inside the (Ti,Nb)B clusters is weak, which means that it is easy for the (Ti,Nb)B phase to break and separate from the matrix in the (Ti,Nb)B cluster [46, 47]. Therefore, the (Ti,Nb)B clusters promote crack initiation and propagation and weaken the strength of the investigated Nb-Ti-ZrB₂ composites. The content of (Ti,Nb)B clusters increases with increasing ZrB_2 volume fraction, resulting in a decreased compressive yield strength. Second, the large residual ZrB_2 particles lead to fewer boundaries to absorb strain energy, and the stress concentration caused by their polygonal shape microstructures also results in the greater possibility of crack initiation and propagation [14]. Therefore, the strength of the Nb-Ti-ZrB₂ composites depends

on the combined influence of the strengthening mechanism caused by (Nb,Ti)B and the weakening mechanism caused by (Ti,Nb)B and ZrB_2 . As shown in Fig.5, it is obvious that the weakening mechanism exceeds the strengthening mechanism, resulting in a decrease in compressive yield strength.

The compressive fracture surfaces of Nb-Ti-ZrB₂ composites are shown in Fig. 9a-c. The stone-like, terrace-type and river pattern morphologies are observed. Large cleavage planes and cleavage steps are also observed and the cleaved cracks propagate along the cleavage plane [48]. Fig. 10a-c show the failure morphologies of the Nb-Ti-ZrB₂ composites after subsection to uniaxial compression tests. It can be observed that the main crack in Nb-Ti-ZrB₂ composites extends at an angle along the compressive direction. Many secondary cracks cause the spallation of fragments. In general, the failure takes place in a pseudoplastic fracture model [49]. At the beginning of the loading process, the cracks in the Nb-Ti-ZrB₂ composites initiate at defects and extend with increasing compressive stress. The increasing stress will generate a shear band [50] in the ductile (Ti,Nb,Zr)ss matrix and the cracks will extend along the shear band. Finally, the failure occurs in the Nb-Ti-ZrB₂ composites together with the existence of some secondary cracks [49].

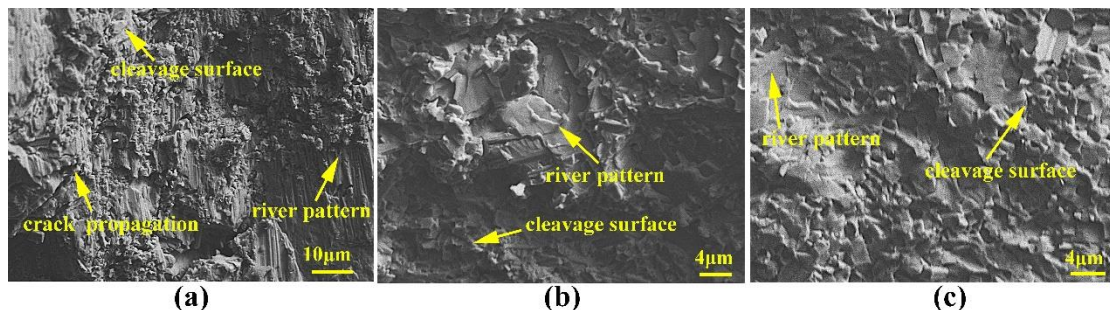


Fig. 9. Fracture surface for (a)Z1, (b)Z2, (c)Z3 after compression test.

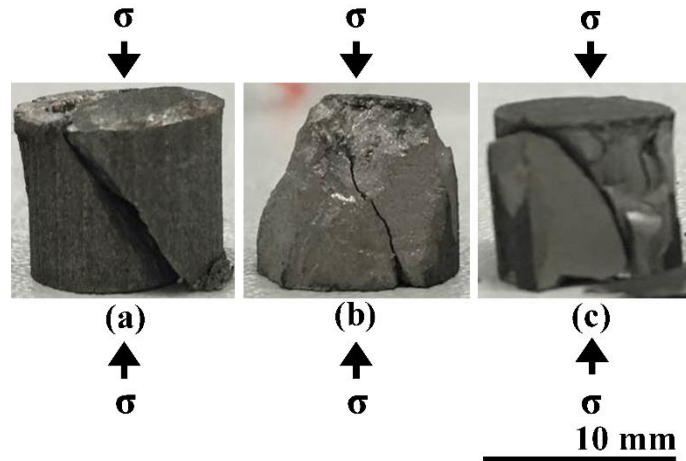


Fig. 10. Failure morphologies for (a)Z1, (b)Z2, (c)Z3 after compression test.

5. Conclusion

Nb-Ti-ZrB₂ metal matrix ceramic composites with ZrB₂ content ranging from 0, 11vol.%, 23vol.% to 36vol.% were successfully hot pressed at 1600°C. The phase, microstructure, mechanical properties and failure processes were investigated. The main conclusions are summarized as follows:

(1) All the Nb-Ti-ZrB₂ composites consist of (Ti,Nb,Zr)ss, Ti-rich (Nb,Ti)B and Nb-rich (Ti,Nb)B phases. The decomposition of ZrB₂ is incomplete when the ZrB₂ content exceeds 36vol.% as there are large residual ZrB₂ particles displayed in the Nb-Ti-36vol.%ZrB₂ composite. The content of niobium and titanium borides increases with increasing ZrB₂ content. The needle-shaped Nb-rich (Ti,Nb)B and the nearly spherical Ti-rich (Nb,Ti)B display in the (Ti,Nb,Zr)ss solid solution matrix.

(2) Three different fracture modes are observed in the Nb-Ti-ZrB₂ composites: quasi-cleavage of the (Ti,Nb,Zr)ss, cleavage of the (Nb,Ti)B and pull-out of the (Ti,Nb)B. The addition of ZrB₂ particles to Nb-Ti alloys causes a decrease in fracture toughness due to ZrB₂ brittle fracture. The (Ti,Nb)B phase can weaken the damage to fracture toughness caused by ZrB₂ particles due

to crack bridging, crack deflection and pull-out toughening mechanisms.

(3) The strength of the Nb-Ti-ZrB₂ composites depends on the combination influence of the strengthening mechanism caused by stiff (Nb,Ti)B and the weakening mechanism caused by (Ti, Nb)B and ZrB₂. The (Nb,Ti)B phase acts as an obstacle to hinder the dislocation motion in the matrix and then enhances the strength of Nb-Ti-ZrB₂ composites. However, the stress concentration around the needle-shaped (Ti, Nb)B phase and large residual ZrB₂ particles readily leads to crack initiation and accelerates the crack propagation with less compatible deformation, resulting in decreased strength. As a result, the strength of Nb-Ti-ZrB₂ composites decreases with increasing ZrB₂ content.

Acknowledgements

This work was supported by the National Natural Science Foundation of China (grant number 11372110); the Fundamental Research Funds for the Central Universities (grant numbers 2019QN030, 2019QN037); and the China Scholarship Council.

Reference

- [1] M.S. Asl, M.G. Kakaoui, S. Noori. Hardness and toughness of hot pressed ZrB₂-SiC composites consolidated under relatively low pressure. *J Alloys Compd* 2015; 619: 481-7.
- [2] F. Wang, J. Li, J. Xu, X. Li, Y. Zhang, H. Wang. Investigation on fracture toughness of aluminum matrix composites reinforced with in situ titanium diboride particles. *J Compos Mater* 2012; 46: 2145-50.
- [3] Y. Tang, X. Guo. Flow softening behavior during hot compression of a Nb-Si based ultrahigh temperature alloy. *J Alloys Compd* 2018; 731: 985-94.
- [4] Y. Guo, L. Jia, B. Kong, H. Zhang, H. Zhang. Microstructure and fracture toughness of

- Nb-Si based alloys with Ta and W additions. *Intermetallics* 2018; 92: 1-6.
- [5] M. Feuerbacher, T. Lienig, C. Thomas. A single-phase bcc high-entropy alloy in the refractory Zr-Nb-Ti-V-Hf system. *Scr Mater* 2018; 152: 40-3.
- [6] V.C. Opini, K.N. Campo, M.G. Mello, E.S.N. Lopes, R. Caram. Effect of partial replacement of V with Nb on phase transformations and mechanical properties of Ti-5553 alloy. *Mater Lett* 2018; 220: 205-8.
- [7] S. Zhiping, G. Jinming, Z. Chen, G. Xiping, T. Xiaodong. Effect of Ti and Al Interaction on Microstructures and Mechanical Properties of the Nb Ti-Si-Al Alloys. *Rare Metal Mat Eng* 2016; 45: 1678-82.
- [8] K. Guan, L. Jia, B. Kong, S. Yuan, H. Zhang. Study of the fracture mechanism of Nb₅₅/Nb₅Si₃ in situ composite: Based on a mechanical characterization of interfacial strength. *Mater Sci Eng A* 2016; 663: 98-107.
- [9] H. Yonglin, J. Lina, J. Zuheng, K. Jin, G. Yueling, S. Jiangbo, Z. Hu. Effect of Sc on the microstructure and room-temperature mechanical properties of Nb-Si based alloys. *Mater Des* 2018; 160: 671-82.
- [10] I. Dinaharan, N. Murugan, S. Parameswaran. Influence of in situ formed ZrB₂ particles on microstructure and mechanical properties of AA6061 metal matrix composites. *Mater Sci Eng A* 2011; 528: 5733-40.
- [11] Z. Shi, H. Wei, H. Zhang, T. Jin, X. Sun, Q. Zheng. Investigation of a hot-pressed Nb-Ti-Al alloy: Mechanical alloying, microstructure and mechanical property. *Mater Sci Eng A* 2016; 651: 869-77.
- [12] D.G. Pan, H.F. Zhang, A.M. Wang, Z.Q. Hu. Enhanced plasticity in Mg-based bulk

metallic glass composite reinforced with ductile Nb particles. *Appl Phys Lett* 2006; 89: 2619041-26190413.

[13] P. Yu, K.B. Kim, J. Das, F. Baier, W. Xu, J. Eckert. Fabrication and mechanical properties of Ni-Nb metallic glass particle-reinforced Al-based metal matrix composite. *Scr Mater* 2006; 54: 1445-50.

[14] Z. Liu, Q. Wang, Y. Gao, Y. Wang, Y. Sun, Y. Gong. Preparation and properties of hot-pressed NbMo-matrix composites reinforced with ZrB₂ particles. *Int J Refract Met Hard Mater* 2017; 68: 104-112.

[15] Q. Wang, Z. Liu, Y. Wang, Y. Sun, Y. Gong. High temperature compression properties of hot-pressed NbMo-matrix composites reinforced with ZrB₂ particles. *Int J Refract Met Hard Mater* 2018; 77: 132-40.

[16] J.F. Bartolomé, M. Díaz, J.S. Moya. Influence of the Metal Particle Size on the Crack Growth Resistance in Mullite-Molybdenum Composites. *J Am Ceram Soc* 2002; 85: 2778-84.

[17] J.S. Moya, M. Díaz, C.F. Gutiérrez-González, L.A. Diaz, R. Torrecillas, J.F. Bartolomé. Mullite-refractory metal (Mo, Nb) composites. *J Eur Ceram Soc* 2008; 28: 479-91.

[18] K.S. Chan. Alloying effects on fracture mechanisms in Nb-based intermetallic in-situ composites. *Mater Sci Eng A* 2002; 329: 513-22.

[19] K. Chan, D. Davidson, D. Anton. Fracture toughness and fatigue crack growth in rapidly quenched Nb-Cr-Ti In situ composites. *Metall Mater Trans A* 1997; 28: 1797-1808.

[20] F. Ye, C. MerCer, W. O. Soboyejo. An Investigation of the Fracture and Fatigue Crack Growth Behavior of Forged Damage-Tolerant Niobium Aluminide Intermetallics. *Metall Mater Trans A* 1998; 29: 2361-74.

- [21] Z. Shi, H. Wei, H. Zhang, D. Wu, T. Jin, X. Sun, Q. Zheng. Investigation of microstructure in hot-pressed Nb-23Ti-15Al alloy. *J Alloys Compd* 2015; 636: 61-6.
- [22] D. B. Borisov, L. V. Artyukh, A. A. Bondar, P. S. Martsenyuk, A. V. Samelyuk, N. I. Tsiganenko, O. S. Fomichov, T. Ya. Velikanova. Titanium-boride eutectic materials: Structure of the Ti-Nb-B alloys and phase equilibria. *Powder Metall Met Ceram* 2007; 46: 58-71.
- [23] B.G. Fu, H.W. Wang, C.M. Zou, Z.J. Wei. Microstructural characterization of in situ synthesized TiB in cast Ti-1100-0.10B alloy. *T Nonferr Metal Sci* 2015; 25: 2206-13.
- [24] R.G. Ding, I.P. Jones, H.S. Jiao. Effect of carbon on the microstructures and mechanical properties of as cast Nb-base alloy. *Mater Sci Eng A* 2008; 485: 92-8.
- [25] G. V. Samsonov, V. S. Neshpor. Investigation of the mutual diffusion of titanium and niobium borides. *Dokl. AN SSSR*: 1955.
- [26] G. V. Samsonov, V. S. Neshpor. Research into the formation of isomorphous boride alloys. *Zh. Fiz. Khim.*; 1955.
- [27] H.B. Feng, D.C. Jia, Y. Zhou, J. Huo. Microstructural characterisation of in situ TiB/Ti matrix composites prepared by mechanical alloying and hot pressing. *Mater Sci Technol* 2004; 9: 1205-10.
- [28] X. Shen, Z. Zhang, S. Wei, F. Wang, S. Lee. Microstructures and mechanical properties of the in situ TiB-Ti metal-matrix composites synthesized by spark plasma sintering process. *J Alloys Compd* 2011; 509: 7692-6.
- [29] Z. Tang, M.J. Kramer, M. Akinc. Evaluation of phase equilibria in the Nb-rich portion of Nb-B system. *Intermetallics* 2008; 16: 255-61.
- [30] B.G. Park, A.G. Crosky, A.K. Hellier. Fracture toughness of microsphere Al₂O₃-Al

- particulate metal matrix composites. *Compos Part B* 2008; 39: 1270-9.
- [31] S.J. Hong, H.M. Kim, D. Huh, C. Suryanarayana, B.S. Chun. Effect of clustering on the mechanical properties of SiC particulate-reinforced aluminum alloy 2024 metal matrix composites. *Mater Sci Eng A* 2003; 347: 198-204.
- [32] P. Poza, J. Llorca. Fracture toughness and fracture mechanisms of Al-Al₂O₃ composites at cryogenic and elevated temperatures. *Mater Sci Eng A* 1996; 206: 183-93.
- [33] J.M. Rice JR. *Inelastic behavior of solids*. New York: McGraw-Hill; 1969.
- [34] S. Zhu, W.G. Fahrenholtz, G.E. Hilmas. Enhanced densification and mechanical properties of ZrB₂-SiC processed by a preceramic polymer coating route. *Scripta Mater* 2008; 59: 123-6.
- [35] Q.B. Nguyen, M. Gupta. Enhancing compressive response of AZ31B magnesium alloy using alumina nanoparticles. *Compos Sci Technol* 2008; 68: 2185-92.
- [36] Y. Tan, C.L. Ma, A. Kasama, R. Tanaka, J.M. Yang. High temperature mechanical behavior of Nb-Mo-ZrC alloys. *Mater Sci Eng A* 2003; 355: 260-6.
- [37] X. Zhang, Y. Zhang, M. Li, Y. Qin, F. Xu, X. He, Y. Li. In-situ precipitated network structure and high-temperature compressive behavior of Nb-Ti-C-B composites. *J Alloys Compd* 2014; 613: 25-32.
- [38] L.M. Peng, Z. Li, H. Li, J.H. Wang, M. Gong. Microstructural characterization and mechanical properties of TiAl-Al₂Ti₄C₂-Al₂O₃-TiC in situ composites by hot-press-aided reaction synthesis.(Report). *J Alloys Compd* 2006; 414: 100-6.
- [39] A. Khan, H.M. Chan, M.P. Harmer, R.F. Cook. Toughening of an Alumina-Mullite Composite by Unbroken Bridging Elements. *J Am Ceram Soc* 2000; 83: 833-40.

- [40] S.Q. Guo. Densification of ZrB₂-based composites and their mechanical and physical properties: A review. *J Eur Ceram Soc* 2009; 29: 995-1011.
- [41] B.S. Li, J.L. Shang, J.J. Guo, H.Z. Fu. In situ observation of fracture behavior of in situ TiBw/Ti composites. *Mater Sci Eng A* 2004; 383: 316-22.
- [42] S. Wei, Z.H. Zhang, F.C. Wang, X.B. Shen, H.N. Cai, S.K. Lee, L. Wang. Effect of Ti content and sintering temperature on the microstructures and mechanical properties of TiB reinforced titanium composites synthesized by SPS process.(Report). *Mater Sci Eng A* 2013; 560: 249-55.
- [43] T. Horiya, T. Kishi. Relationship between fracture toughness and crack extension resistance curves (R curves) for Ti-6Al-4V alloy. *J Metall Mater Trans A* 1998; 29: 781-789.
- [44] M. Sygnatowicz ; Raymond A. Ciolek; Dinesh K. Shetty. ζ - Ta₄C_{3-x}: A High Fracture Toughness Carbide with Rising- Crack- Growth- Resistance (R- Curve) Behavior. *J Am Ceram Soc* 2015; 98: 2601-2608.
- [45] X. Zhang, X. He, C. Fan, Y. Li, G. Song, Y. Sun, J. Huang. Microstructural and mechanical characterization of multiphase Nb-based composites from Nb-Ti-C-B system. *Int J Refract Met Hard Mater* 2013; 41: 185-90.
- [46] Y. Yang, L. Chenglin, F. Yanyan, H. Songxiao, Y. Wenjun. Effect of Trace Boron Addition on Microstructure and Properties of as-Cast Ti-6Al-4V Alloy. *Rare Metal Mat Eng* 2014; 43: 2908-11.
- [47] Z.Y. Hu, X.W. Cheng, S.L. Li, H.M. Zhang, H. Wang, Z.H. Zhang, F.C. Wang. Investigation on the microstructure, room and high temperature mechanical behaviors and strengthening mechanisms of the (TiB+TiC)/TC4 composites. *J Alloys Compd* 2017; 726:

240-53.

[48] Z. Li, L. Xu, S. Wei, C. Chen, F. Xiao. Fabrication and mechanical properties of tungsten alloys reinforced with c-ZrO₂ particles. *J Alloys Compd* 2018; 769: 694-705.

[49] Z. Li, L.M. Peng. Microstructural and mechanical characterization of Nb-based in situ composites from Nb-Si-Ti ternary system. *Acta Mater* 2007; 55: 6573-85.

[50] C.K. Meyers MA. *Mechanical behavior of materials*. Englewood Cliffs: NJ: Prentice-Hal; 1999.

Journal Pre-proof

♥ (Ti,Nb,Zr)ss ▽TiB ♣NbB ◇ZrB₂

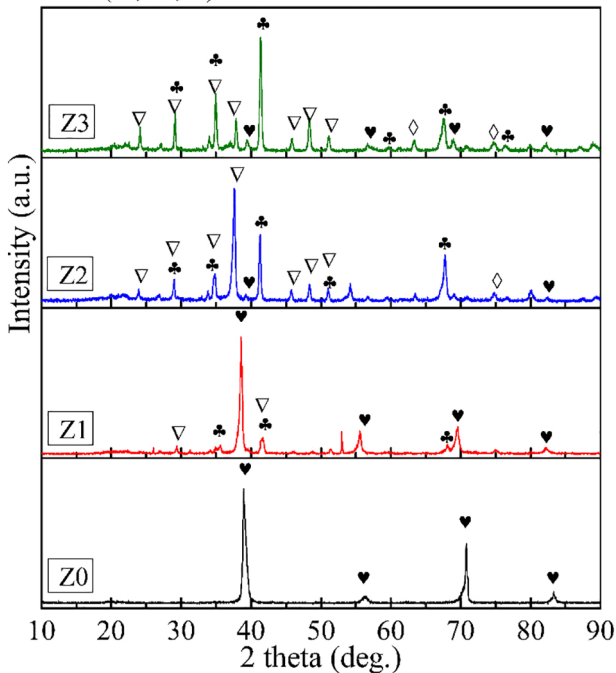


Figure 1

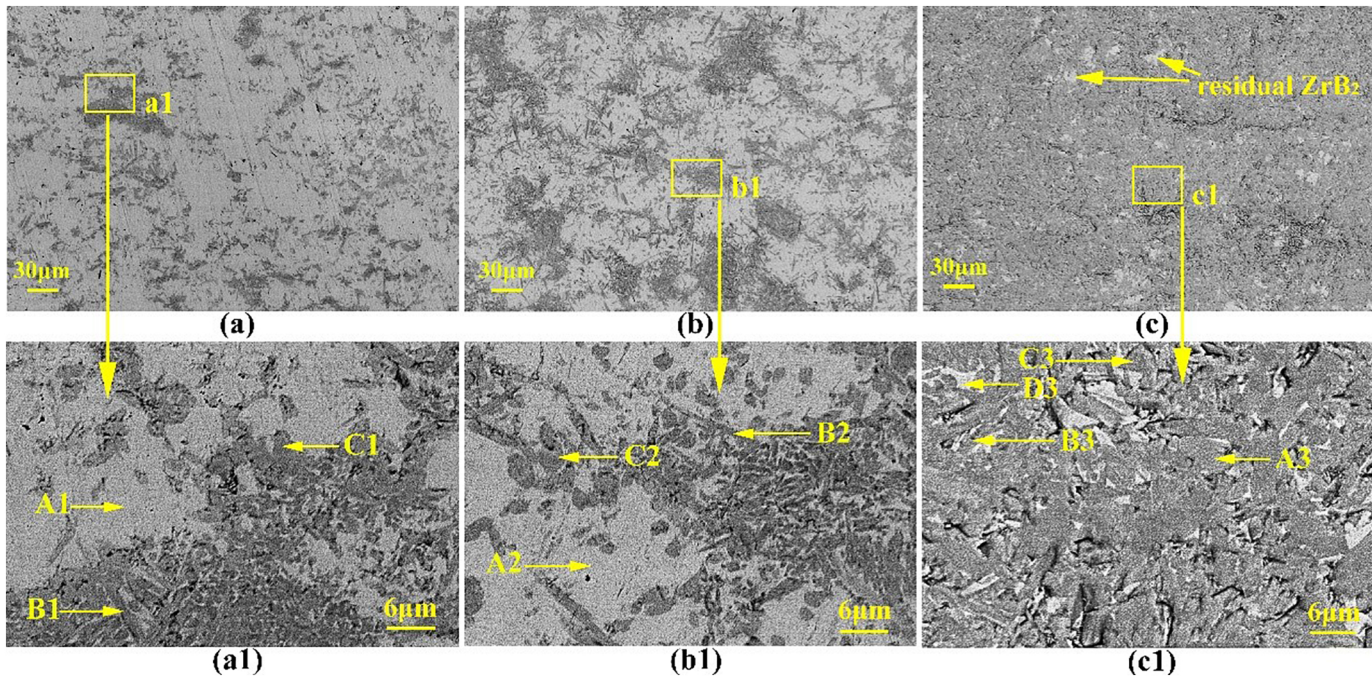


Figure 2

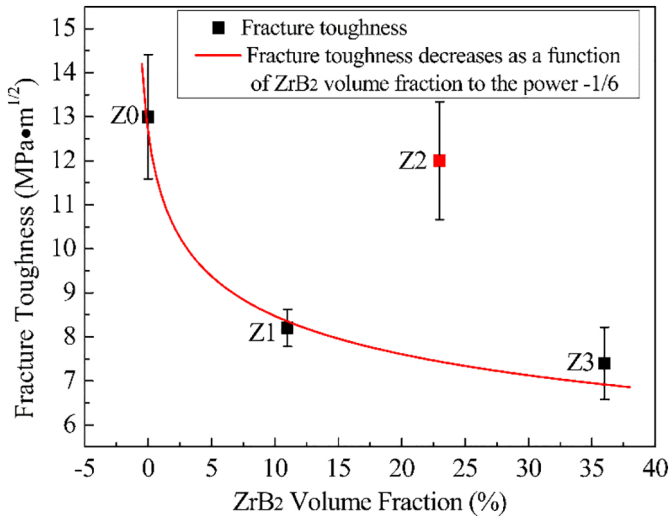


Figure 3

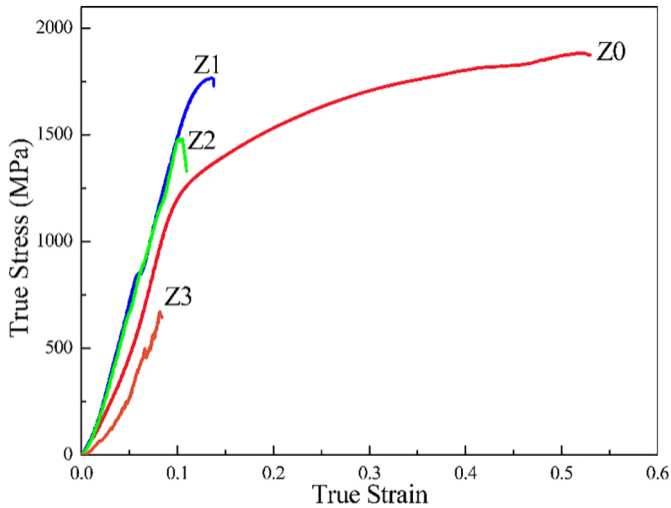


Figure 4

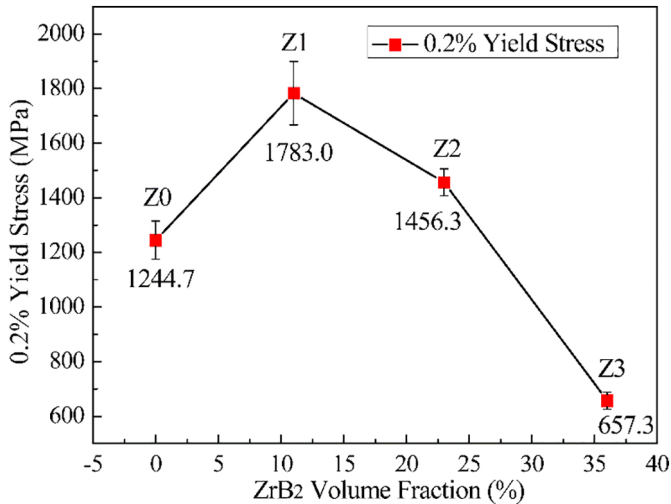
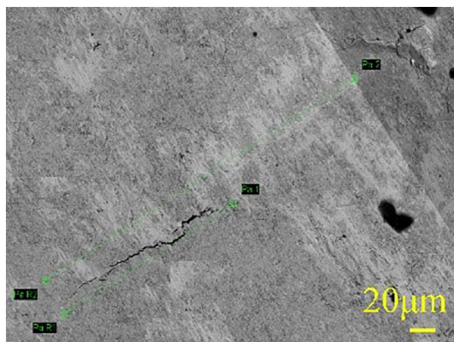
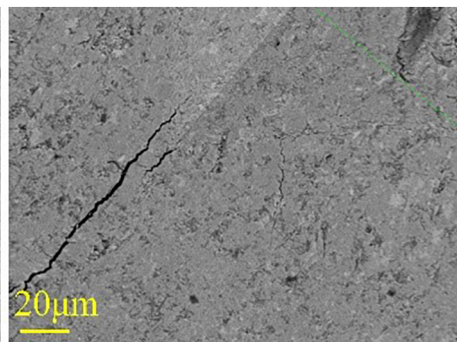


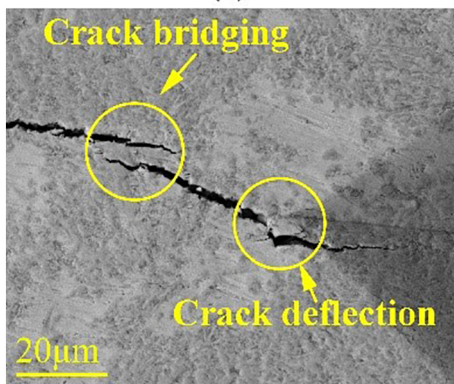
Figure 5



(a)



(b)

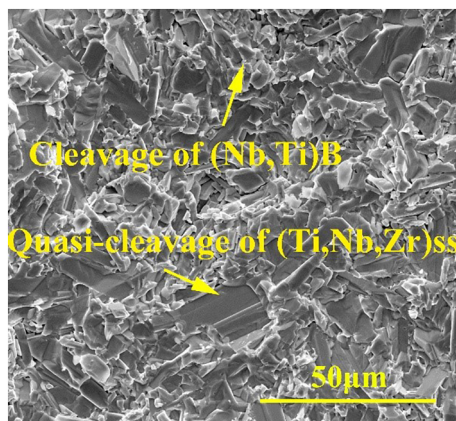


(c)

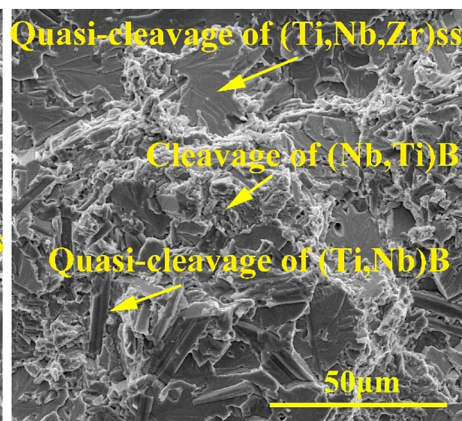


(d)

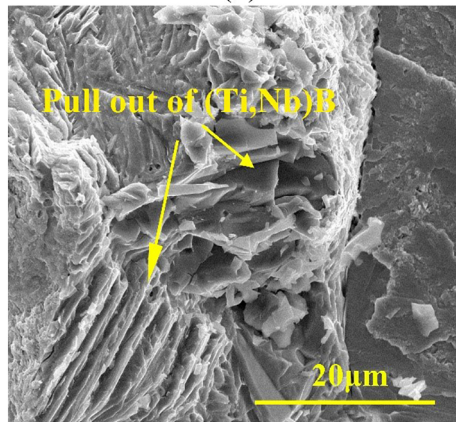
Figure 6



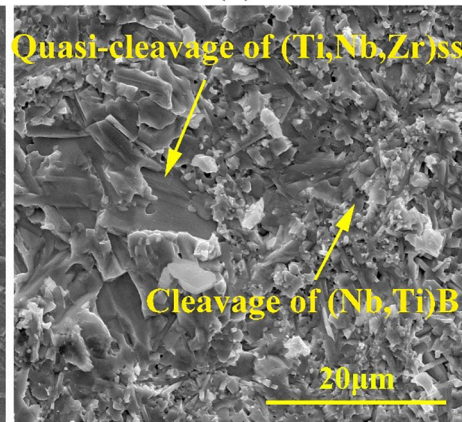
(a)



(b)



(c)



(d)

Figure 7

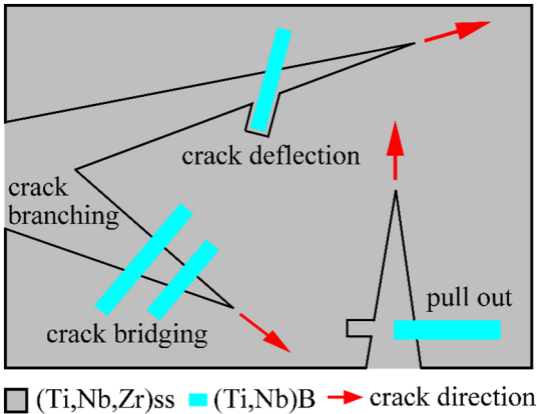
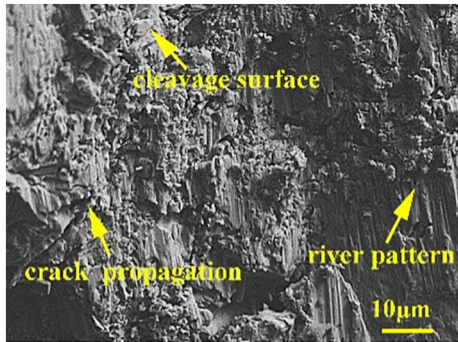
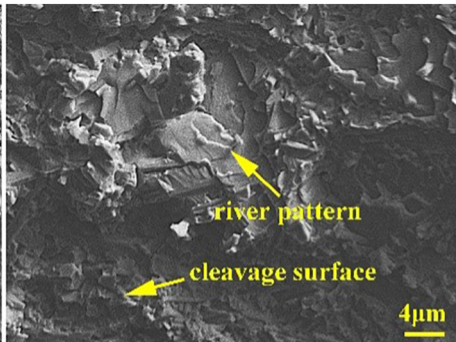


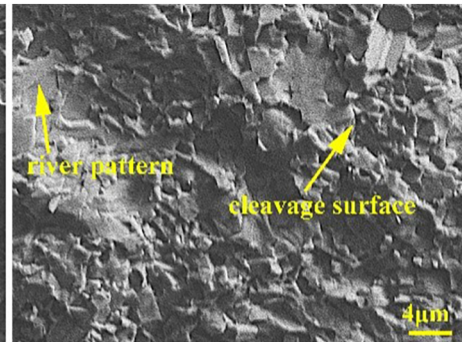
Figure 8



(a)



(b)



(c)

Figure 9

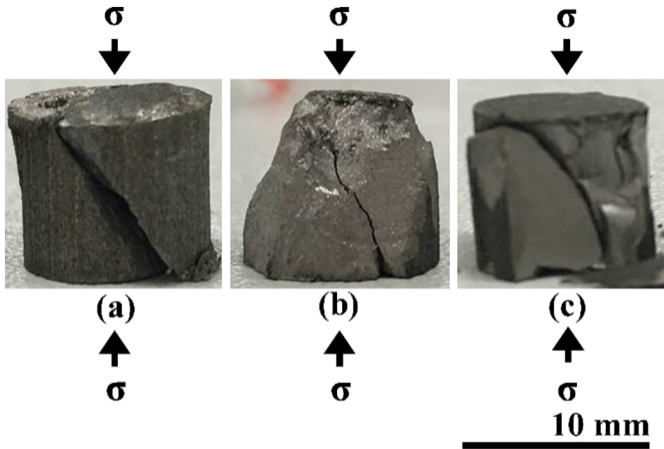


Figure 10